

Radio Resource Management for Cellular-Connected UAV: A DRL Solution

Yuanjian Li and A. Hamid Aghvami, *Fellow, IEEE*

Abstract

Integrating unmanned aerial vehicles (UAVs) into the existing cellular networks faces lots of challenges, in which one of the most striking concerns is how to adopt UAVs into cellular networks with less adverse effects on ground user equipments (UEs). In this paper, a cellular-connected UAV network is considered, where multiple UAVs receive messages from terrestrial BSs in the down-link, while BSs are serving ground users in their cells. To enhance wireless transmission quality for UAVs while protecting ground UEs from being interfered, a joint time-frequency resource block (RB) and beamforming optimization problem minimizing the ergodic outage duration (EOD) of UAV is investigated. To solve the proposed radio resource management problem, a deep reinforcement learning (DRL) solution is proposed, where deep double duelling Q network (D3QN) and twin delayed deep deterministic policy gradient (TD3) are invoked to deal with RB allocation in discrete action domain and beamforming design in continuous action regime, respectively. The hybrid D3QN-TD3 solution is applied to solve the outer MDP and the inner MDP interactively so that it can achieve the sub-optimal result for the considered optimization problem. Simulation results have illustrated the effectiveness of the proposed hybrid D3QN-TD3 algorithm, compared to exhaustive/random search based benchmarks.

Index Terms

Unmanned aerial vehicle (UAV), cellular networks, deep reinforcement learning, radio resource management, interference management, beamforming.

Yuanjian Li and A. Hamid Aghvami are with Centre for Telecommunications Research (CTR), King's College London, London WC2R 2LS, U.K. (e-mail: {yuanjian.li, hamid.aghvami}@kcl.ac.uk)

This work has been submitted to the IEEE for possible publication. Copyright may be transferred without notice, after which this version may no longer be accessible.

I. INTRODUCTION

Typically, unmanned aerial vehicles (UAVs) are communicating with ground transceivers through simple point-to-point channels over unlicensed spectrum, resulting in constrained transmission performance [1]. To circumvent this, cellular-connected UAV communication is deemed as a promising solution, where base stations (BSs) in terrestrial cellular networks are leveraged to achieve more satisfactory ground-to-air (G2A) transmission quality [2], [3]. Unfortunately, the existing cellular networks are exclusively established for serving ground user equipments (GUEs), barely considering aerial UEs. Specifically, antennas at BSs in current cellular networks are conventionally down-tilted towards the ground for mitigating terrestrial inter-cell interferences (ICIs), which means that UAVs can only be served via the side-lobes and satisfactory G2A connections cannot be guaranteed in general [4], [5]. On the perspective of forthcoming 5G-beyond or 6G cellular networks, the main serving objects are still GUEs, raising that finding a proper way of involving UAVs into cellular networks without posing negative impacts on terrestrial transmissions is inherently of importance. In fact, integrating drones into the existing cellular networks has already been one of the most important research directions, which is believed to further release the potentials of drones in terms of reliability, coverage and throughput. Unlike terrestrial cellular transmissions where non-line-of-sight (NLoS) pathloss appears more frequently, the first significant difference introduced by drones is that line-of-sight (LoS) link occurs more likely in G2A communications [6]–[10], which plays the role as a double-edge blade. On one hand, LoS-dominant G2A links can help relieve the sufferance of severe multi-path fading, shadowing and pathloss, which are very common "illnesses" in terrestrial transmissions due to the existence of blockages, e.g., buildings and trees. On the other hand, it may make drones generate stronger interferences (or suffer more severe interferences) to (or from) BSs in the up-link (or the down-link) transmissions. Besides, drones can cover larger region for data transmissions due to their high flying altitudes, then greater *macro-diversity gain* can usually be achieved because more BSs can cooperate to enhance G2A communication qualities in terms of throughput and reliability. Unfortunately, more co-channel interfering sources for the drones in the down-link might be involved as well (or, UAVs can act as the interferers to more GUEs in the up-link). Therefore, interference coordination issue for cellular-connected UAV networks is more intricate and must be seriously treated.

Various interference management strategies have been investigated in the literature for ter-

terrestrial cellular transmission scenario, e.g., inter-cell interference coordination (ICIC) [11], [12], cognitive beamforming [13] and coordinated multipoint (CoMP) communications [14]. However, they are most likely ineffective to handle more sophisticated interfering environment caused by UAVs with LoS-dominant G2A links and larger coverage. Therefore, interference management approaches that are adaptive to cellular-connected UAV networks should be delicately designed to achieve efficient spectrum sharing with coexisting GUEs. Up to date, there exist several related works devoted to offering interference management approaches for cellular-connected UAV networks [1], [2], [15], [16]. Chandhar *et al.* [2] leveraged multiple-input multiple-output (MIMO) technique to deal with interference coordination problem of single-antenna UAV swarms served by a multiple-antenna BS. Senadhira *et al.* [15] studied the impacts of UAV's trajectory and altitude for up-link non-orthogonal multiple access (NOMA) cellular-connected UAV network, in which ICI issue was dealt with NOMA technique. However, protecting the GUEs located in current cell or other cells within the coverage of UAVs was not considered in these works, which may significantly deteriorate the transmission performance of potential co-channel GUEs. Fortunately, some recent literature took care of interference control issue while protecting GUEs in cellular-connected UAV networks [1], [16]. Liu *et al.* [1] proposed a new cooperative interference cancellation strategy for multi-beam cellular-connected UAV up-link transmissions, in which co-channel interference elimination and sum-rate maximization were investigated with the help of transmit beamforming design. Mei *et al.* [16] studied interference mitigation issue in up-link communications from a UAV to BSs, where weighted sum-rate of the UAV and GUEs was maximized via jointly optimizing up-link cell association and power allocation. However, these works contain practical limitations. First, they both assumed fixed-location UAV in their considered model, without involving UAV's mobility. Second, the G2A channel models they applied are based on either oversimplified free-space pathloss channel model or slightly advanced probabilistic LoS channel model. It is worth noting that probabilistic G2A channel model is statistical, which means that it can only reflect G2A pathloss gain in an expected manner without considering local building distribution where UAVs are actually deployed [17]. Last but not least, traditional optimization-based problems (e.g. those in [1], [16]) are highly non-convex and hard to be tackled efficiently, even with adequate information of needed evaluation factors.

Motivated by the above observations, radio resource management issue on interference coordination and beamforming design in down-link cellular-connected UAV networks is investigated in this paper. It is worth noting that the terrestrial transmissions between GUEs and BSs are

protected to be not contaminated by the down-link G2A channels. The main contributions of this paper can be concluded as follows.

- A joint time-frequency resource block (RB) allocation and beamforming design optimization problem is formulated to minimize the ergodic outage duration (EOD) of UAV, for arbitrary given trajectory. Specifically, the RB allocation is utilized to assign proper RB resource to UAVs while insuring that the terrestrial transmissions are not violated by the potential co-channel interferences generated from BSs aligned to serve UAVs. To enhance the quality of received signals at UAVs after RB allocation, transmit beamforming design is invoked in the presence of imperfect G2A channel estimation.
- To deal with the difficulty of traditional optimization-based methods solving the proposed EOD minimization problem, a deep reinforcement learning (DRL) [18], [19] aided solution is proposed via mapping the proposed EOD minimization problem into an outer Markov decision process (MDP) and an inner MDP. The outer MDP reflects the dynamic RB possession environment at BSs, while the inner MDP tracks the corresponding small-scale fading characteristics. The outer MDP contains discrete action space (i.e., RB indices), which is tackled by invoking deep double duelling Q network (D3QN), while the continuous action space (i.e., beamforming vectors) in the inner MDP is dealt with twin delayed deep deterministic policy gradient (TD3) approach. The proposed hybrid D3QN-TD3 algorithm can optimize EOD performance for UAVs via interactively interacting with the outer and inner environments, of which the D3QN and TD3 agents are able to offer independent EOD performance gains.
- In contrast to the majority of related literature adopting statistical G2A channel model (e.g., probabilistic G2A channel model), LoS/NLoS G2A pathloss is determined via checking potential blockages between UAV and BSs in this paper, according to one realization of local building distribution suggested by the International Telecommunication Union (ITU) [20]. The considered G2A channel model is more practical than its statistical counterpart which can only reflect average pathloss gain over large number of similar building distribution realizations because building distribution in local area remains unchanged in practice.

II. SYSTEM MODEL

In this paper, radio resource management problem of RB allocation and beamforming design for down-link cellular-connected UAV network is considered, where a set $\mathcal{B} = \{1, \dots, B\}$ of B

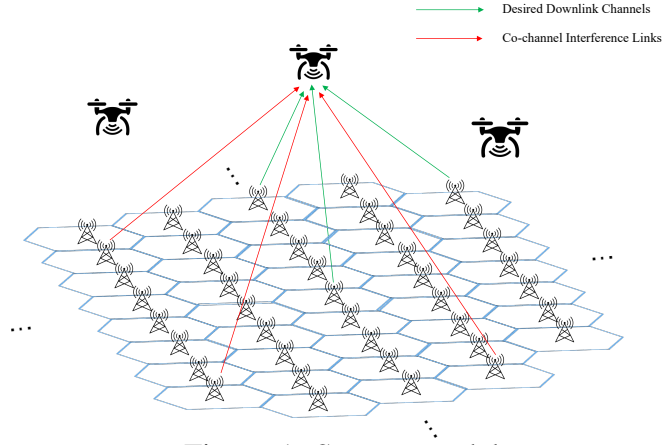


Figure 1: System model

terrestrial BSs serves a set $\mathcal{U} = \{1, \dots, U\}$ of U drone UEs (DUEs) and a set $\mathcal{G} = \{1, \dots, G\}$ of G GUEs using a set $\mathcal{K} = \{1, \dots, K\}$ of K RBs at each BS, within a given subregion (e.g., Fig. 1) of cellular network. Each DUE is assumed to equip single antenna for receiving wireless information and so as each GUE, while all the terrestrial BSs employ antenna array for message emitting. Specifically, each terrestrial BS $b \in \mathcal{B}$ possesses M antennas, serving g_b GUEs with orthogonal RBs (so there does not exist intra-cell interferences within each cell), where $g_b \geq 1, \forall b \in \mathcal{B}$ and $\sum_{b=1}^B g_b = G$. Different from terrestrial transmission scenario, DUEs fly in the sky at relatively high altitudes, resulting in higher probability of achieving LoS-dominant links from BSs. Thus, DUEs are able to connect with more BSs within their wireless coverage, which is a distinguishable feature compared to terrestrial transmissions. However, this characteristic may not only induce more and stronger desired signals but also result in richer co-channel interferences. To practically reflect the aforementioned double-edge blade feature, each DUE is considered to be associated with at least one BS when possible, taking advantage of macro-diversity gain from terrestrial BSs. Unfortunately, the assigned RB for a DUE might be already occupied by some GUEs due to heavy frequency reuse in cellular networks, severely interfering the DUE via LoS-dominant channels. Therefore, RB allocation plays an important role in the considered cellular-connected UAV network. Besides, after RB assignment for a DUE, wireless transmission performance can be enhanced via invoking transmit beamforming technique at the corresponding serving BSs. Note that we do not consider transmit power control

strategy at each BS, and thus we fix $P_b = P$ for all terrestrial BSs.¹

The 3-dimensional (3D) locations of each DUE, each ground BS and each GUE are denoted as $\vec{q}_u = (x_u, y_u, h_u)$, $\vec{q}_b = (x_b, y_b, z_b)$ and $\vec{q}_g = (x_g, y_g, 0)$, respectively. For simplicity and without loss of generality, the flying altitude of each DUE is assumed universally as $h_u = h$ and the height of each BS's antenna is set identically as $z_b = z$, where $h \gg z$ always holds in the considered model. Each DUE is supposed to reach its destination $\vec{q}_u(D)$ from predefined initial location $\vec{q}_u(I)$ with time duration T_u .²

For clarity, the considered subregion is formulated as a cubic sphere specified by $[x_{lo}, x_{up}] \times [y_{lo}, y_{up}] \times [z_{lo}, z_{up}]$, where the subscripts "lo" and "up" represent the lower and upper boards of this 3D airspace, respectively. Furthermore, the coordinate of arbitrary DUE u at time $t \in [0, T_u]$ should locates in the range of $\vec{q}_{lo} \preceq \vec{q}_u(t) \preceq \vec{q}_{up}$, where $\vec{q}_{lo} = (x_{lo}, y_{lo}, z_{lo})$, $\vec{q}_{up} = (x_{up}, y_{up}, z_{up})$ and \preceq denotes the element-wise inequality. The start and final locations of each DUE are indicated as $\vec{q}_u(0) = \vec{q}_u(I)$ and $\vec{q}_u(T_u) = \vec{q}_u(D)$, respectively. Therefore, the trajectory of each DUE u can be fully traced by $\vec{q}_u(t), \forall t \in [0, T_u]$.

A. The RB Allocation Criterion

To properly manage ICIs among G GUEs, the following RB assignment criterion is adopted at all BSs. The set $\mathcal{TI}_b(p)$ is defined to denote the first p -tier BSs that encompass a specific BS $b \in \mathcal{B}$ in the considered model, where $1 \leq p \leq 3$ and $\mathcal{TI}_b(p)$ includes this focused BS. When arbitrary RB has been assigned to any GUE in the serving cells of BSs from $\mathcal{TI}_b(p)$, the focused BS b should avoid allocating this RB to other GUEs in its corresponding cell.³ To ensure that the total RB resource is sufficient for all GUEs in cells of BSs from $\mathcal{TI}_b(p)$, the constraint $\sum_{b \in \mathcal{TI}_b(p)} g_b \leq K$ should hold, where $card(\mathcal{TI}_b(p)) = 3p^2 + 3p + 1$ and $card(\cdot)$

¹Transmit power control is indeed an important approach for interference management in cellular networks. In our considered model, it is straightforward to infer that all BSs should communicate with their paired DUEs using maximum transmit power. Besides, all the occupied BSs are supposed to apply their minimum transmit power to reduce the level of co-channel interference to DUEs, which inevitably deteriorates the transmission quality for their severing GUEs. Therefore, to tackle this dilemma, we fix the transmit powers of all considered BSs as a constant P .

²For specific DUE $u \in \mathcal{U}$, the flying duration T_u is determined by its trajectory and velocity. Besides, the RB allocation and beamforming design are independent of trajectories, which means that the proposed solution is suitable for arbitrary trajectory. Therefore, trajectory planning task is not included in this paper.

³In the case of sufficiently large p , the ICIs among all GUEs become ignorable, thanks to sufficient frequency reuse and severe terrestrial pathloss.

indicates the cardinality of a set. In this regard, the focused BS b cannot generate any ICIs to GUEs in the serving cells of BSs from $\mathcal{T}\mathcal{I}_b(p)$. For GUEs outside the serving cells of BSs from $\mathcal{T}\mathcal{I}_b(p)$, the potential ICIs caused by the focused BS b are assumed to be negligible, due to severe terrestrial NLoS pathloss and shadowing. For each possible RB k , some BSs may already occupy it to serve GUEs in their corresponding cells. These BSs are recognized as the occupied BSs, which are denoted by the occupied BS set $\mathcal{B}_o^k \subset \mathcal{B}$. Furthermore, the set $\hat{\mathcal{B}}_o^k = \mathcal{B} \setminus \mathcal{B}_o^k$ includes all the potential BSs, where the RB k is idle. For a specific RB k assigned to serve a DUE, the corresponding associated BSs come from the potential set $\hat{\mathcal{B}}_o^k$, while all the non-associated co-channel interferences root from the occupied set \mathcal{B}_o^k . For a DUE u associated with a RB k , it is supposed to be paired with all BSs in the potential set $\hat{\mathcal{B}}_o^k$, to take the advantage of macro-diversity gain. However, this may generate additional ICIs to GUEs in the serving cells of BSs from $\mathcal{T}\mathcal{I}_{b \in \hat{\mathcal{B}}_o^k}(p)$. To avoid ICIs attenuating the receiving quality of existing GUEs over the same RB, a potential BS $b \in \hat{\mathcal{B}}_o^k$ can be allowed to pair DUE if and only if there are no other BSs applying RB k in its first p -tier neighbours, i.e.,

$$\hat{\mathcal{B}}_o^k \cap \mathcal{T}\mathcal{I}_{b \in \hat{\mathcal{B}}_o^k}(p) = \emptyset. \quad (1)$$

Then, the available BS set $\check{\mathcal{B}}_o^k \subset \hat{\mathcal{B}}_o^k$ is defined to denote the potential BSs satisfying (1).

B. Channel Models

In contrast to terrestrial transmission between BS and GUE (denoted as B2G thereafter), wireless links between BS and DUE (denoted as B2U thereafter) have higher probability experiencing LoS pathloss [21]. In this subsection, channel model of the considered cellular-connected UAV network will be introduced.

1) *B2G Channel Model*: The B2G channel may include the large-scale fading caused by NLoS-dominated pathloss and corresponding small-scale fading exponent in practice. In this paper, we consider the down-link interference management problem, where the terrestrial transmissions could affect the B2U communication quality as a part of co-channel interferences. This is because the occupied BSs may apply some channel-aware precoding techniques to enhance their transmissions with corresponding GUEs. Specifically, the terrestrial small-scale fading component is denoted as $\vec{h}_{bg} \in \mathbb{C}^{1 \times M}$, $\forall b \in \mathcal{B}, g \in \mathcal{G}$. Note that the modelling of \vec{h}_{bg} is trivial for this paper, which means that \vec{h}_{bg} can take form of any practical and feasible small-scale fading model, e.g., Rayleigh fading channel. In the section of numerical results, an example of terrestrial small-scale fading will be specified to perform the simulation.

2) *B2U Channel Model*: Probabilistic B2G pathloss model is widely applied to characterize wireless pathloss between BS and DUE in current literature, where LoS and NLoS channels are considered separately with different occurrence probabilities. According to 3GPP urban-macro (UMa) channel model [22], the expected B2U pathloss in dB can be expressed as $PL_{bu} = Pr_{LoS}PL_{LoS} + Pr_{NLoS}PL_{NLoS}$, where Pr_{LoS} represents the occurrence probability of LoS link, $Pr_{NLoS} = 1 - Pr_{LoS}$ indicates that of NLoS channel, and PL_{LoS} and PL_{NLoS} denote the pathlosses for LoS and NLoS links, respectively. Specifically, we have

$$Pr_{LoS} = \begin{cases} \min\{\frac{\varepsilon_1}{r_{bu}}, 1\} \left[1 - \exp\left(-\frac{r_{bu}}{\varepsilon_2}\right)\right] + \exp\left(-\frac{r_{bu}}{\varepsilon_2}\right), & 22.5\text{m} < h \leq 100\text{m} \\ 1, & 100\text{m} < h \leq 300\text{m} \end{cases}, \quad (2)$$

$$PL_l = \begin{cases} 28.0 + 22 \log_{10}(d_{bu}) + 20 \log_{10}(f_c), & l = \text{LoS} \\ -17.5 + [46 - 7 \log_{10}(h)] \log_{10}(d_{bu}) + 20 \log_{10}\left(\frac{40\pi f_c}{3}\right), & l = \text{NLoS} \end{cases}, \quad (3)$$

in which $r_{bu} = \sqrt{d_{bu}^2 - h^2}$, $\varepsilon_1 = \max\{460 \log_{10}(h) - 700, 18\}$, $\varepsilon_2 = 4300 \log_{10}(h) - 3800$, f_c represents the carrier frequency and $d_{bu} = \|\vec{q}_u - \vec{q}_b\|_2$ calculates the Euclidean distance between DUE u and ground BS b . Since the proposed design on beamforming vectors aims to be adaptive to arbitrary small-scale fading environment, we denote $\vec{h}_{bu} \in \mathbb{C}^{1 \times M}, \forall b \in \mathcal{B}, u \in \mathcal{U}$ as the small-scale fading component for B2U channels and an example of specific B2U small-scale fading model will be discussed in the numerical result section.

To practically reflect the characteristics of B2U channels in the considered subregion, one realization of the statistical model suggested by the ITU is generated to formulate the building distribution (including structures' 2D locations on the ground and their corresponding heights). There are three key parameters in the ITU building distribution model: 1) $\hat{\alpha}$ indicates the ratio of land region covered by buildings to the total land area; 2) $\hat{\beta}$ represents the mean of buildings per unit area; and 3) $\hat{\gamma}$ determines the distribution of building heights, which is typically following Rayleigh distribution with mean $\hat{\gamma} > 0$. Note that the B2U pathlosses are modelled and tracked in terms of average large-scale channel gain via calculating the occurrence probabilities of LoS/NLoS links as depicted in (2), in the vast majority of related literature. This kind of approach is more mathematically tractable, however, it can only reflect the ergodic characteristics of B2U channels over many realizations of building distribution. On the contrary, in this paper, the occurrences of LoS/NLoS links are alternatively tracked via checking whether the line of B2U channel is blocked or not by any building, given one realization of ITU building

distribution model.⁴ Then, the corresponding type of large-scale pathloss can be determined for each time of B2U channel regeneration. Fig. 2 illustrates the considered one realization of local building distribution in this paper, where 25 building clusters and 37 BSs are depicted in a square subregion with side length $D = 3$ km, road width $\hat{D} = 0.02$ km, $\hat{\alpha} = 0.3$, $\hat{\beta} = 103$ buildings/km² and $\hat{\gamma} = 20$ m. With these parameter settings, the total amount of buildings is $\hat{\beta}D^2 = 927$ and the expected size of each building is $\hat{\alpha}/\hat{\beta} \approx 0.003$ km². Besides, the maximum height of buildings is clipped to be under 70 m, and the locations of BSs are presented by white asterisks in Fig. 2(a).

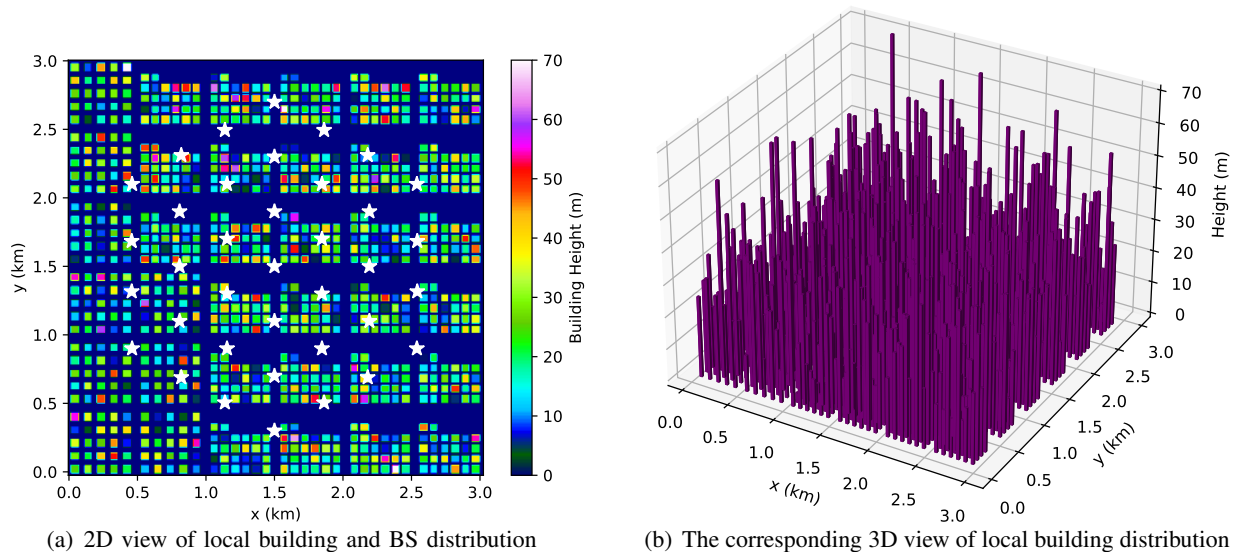


Figure 2: The considered building distribution

C. SINR at DUE

Denote $C_u^k(t) \in \{0, 1\}$ as the RB association indicator which means that DUE u is occupying RB k at time t when $C_u^k(t) = 1$, and $C_u^k(t) = 0$ otherwise. Each DUE is assumed to occupy at most one single RB each time⁵, then we have $\sum_{k=1}^K C_u^k(t) \leq 1$.

If RB k is feasible to be assigned to DUE u , i.e., $C_u^k(t) = 1$, it has to satisfy the RB assignment criterion presented in Subsection II-A. Then, all BSs in the potential set $\hat{\mathcal{B}}_o^k$ meeting the regulation (1), i.e., $b \in \check{\mathcal{B}}_o^k$, are recognized as the available BSs for DUE u , to take the advantage of macro-diversity gain. Besides, all BSs $b \in \mathcal{B}_o^k$ occupying the selected RB k should

⁴Note that our approach is more practical because the building distribution of a subregion in real world can hardly vary over time (say, days even years).

⁵In this paper, we focus on the scenario in which each DUE can only occupy one single RB each time. Integrating more sophisticated RB allocation approaches might be considered in our future works.

be classified as the source of co-channel ICIs. Thus, the received signal of DUE u over RB k at time t can be given by

$$y_u^k(t) = C_u^k(t) \left[\sum_{b \in \check{\mathcal{B}}_o^k} \sqrt{10^{-\frac{\text{PL}_l}{10}}} \vec{h}_{bu} \vec{w}_{bu} x_u(t) + \sum_{b \in \mathcal{B}_o^k} \sqrt{10^{-\frac{\text{PL}_l}{10}}} \vec{h}_{bu} \vec{w}_{bg} x_{bg}(t) + n_u^k \right], \quad (4)$$

where $\vec{w}_{bu} \in \mathbb{C}^{M \times 1}$ indicates the transmit beamforming vector at BS $b \in \check{\mathcal{B}}_o^k$ for DUE u , $\vec{w}_{bg} \in \mathbb{C}^{M \times 1}$ represents the transmit beamforming vector at BS $b \in \mathcal{B}_o^k$ for corresponding GUEs, $x_u(t) \sim \mathcal{CN}(0, P)$ is the intended message from BS b to DUE u , $x_{bg}(t) \sim \mathcal{CN}(0, P)$ implies the signal for GUEs, and $n_u^k \sim \mathcal{CN}(0, \sigma^2)$ denotes the received additive complex Gaussian noise (AWGN) at DUE u . Note that the explicit type of large-scale fading between BS b and DUE u at time t , i.e., $l = \{\text{LoS}, \text{NLoS}\}$, can be determined via checking possible blockages according to the considered one realization of local building distribution mentioned in Subsection II-B2. Taking the advantages of macro-diversity gain, all signals from the associated BS $b \in \check{\mathcal{B}}_o^k$ are recognized as the legitimate in-phase information and thus can be added constructively at DUE u . The channel state information (CSI) of $\vec{h}_{bu}, b \in \check{\mathcal{B}}_o^k$ and $\vec{h}_{bg}, b \in \mathcal{B}_o^k$ can be estimated via widely-applied MMSE-based methods. Unfortunately, the CSI can not be perfectly obtained in practice, due to estimation error and/or feedback delay [23], [24]. Therefore, the imperfect CSI model on $\vec{h}_{bu}, b \in \check{\mathcal{B}}_o^k$ is considered in this paper, expressed as

$$\vec{h}_{bu} = \sqrt{\rho} \vec{\hat{h}}_{bu} + \sqrt{1 - \rho} \vec{\Delta}, \quad (5)$$

where $\vec{\hat{h}}_{bu}$ indicates the estimated CSI, $\vec{\Delta} \sim \mathcal{CN}(0, \mathbf{I})$ denotes the CSI estimation error vector and $\rho \in [0, 1]$ is the correlation coefficient between \vec{h}_{bu} and $\vec{\hat{h}}_{bu}$. For an impractical case $\rho = 1$, i.e., perfect CSI availability at the available BSs, maximum ratio transmission (MRT) precoding $\vec{w}_{bu} = \vec{h}_{bu}^\dagger / \|\vec{h}_{bu}\|$ is obviously the optimal option. However, for practical consideration, \vec{w}_{bu} should be designed according to the estimated CSI $\vec{\hat{h}}_{bu}$, whose performance will be inevitably deteriorated due to the existence of CSI estimation error. Then, the instantaneous signal-to-interference-plus-noise-ratio (SINR) of DUE u at time t can be calculated as

$$\Gamma_u(t) = \sum_{k=1}^K \frac{C_u^k(t) \sum_{b \in \check{\mathcal{B}}_o^k} P 10^{-\frac{\text{PL}_l}{10}} |\vec{h}_{bu} \vec{w}_{bu}|^2}{I_u^k(t) + \sigma^2}, \quad (6)$$

where $I_u^k(t) = \sum_{b \in \mathcal{B}_o^k} P 10^{-\frac{\text{PL}_l}{10}} |\vec{h}_{bu} \vec{w}_{bg}|^2$ means the ICIs introduced by the co-channel BSs in the occupied set \mathcal{B}_o^k .

D. Problem Formulation

It is clear that the received SINR of DUE u at time t , i.e., formula (6), is a random variable because of the randomness introduced by small-scale fading \vec{h}_{bu} and \vec{h}_{bg} , as well as the RB allocation. Specifically, the RB allocation affects $\Gamma_u(t)$ in terms of how many available BSs and interfering BSs will be involved, i.e., $\text{card}(\check{\mathcal{B}}_o^k)$ and $\text{card}(\mathcal{B}_o^k)$, respectively. Then, with given RB allocation, the transmit beamforming vector $\vec{\omega}_{bu}$ should be designed to adapt to the small-scale fading \vec{h}_{bu} . Therefore, the corresponding transmission outage probability (TOP) can be formulated as a function of $C_u^k(t)$ and $\vec{\omega}_{bu}$, given by

$$TOP_u\{C_u^k(t), \vec{\omega}_{bu}\} = \Pr[\Gamma_u(t) < \Gamma_{th}], \quad (7)$$

where \Pr outputs the probability calculated with respect to (w.r.t.) the aforementioned small-scale fading and B2U transmit beamforming vector, with given RB allocation. Then, the EOD of DUE u travelling with trajectory $\vec{q}_u(t), \forall t \in [0, T_u]$ from $\vec{q}_u(I)$ to $\vec{q}_u(D)$ can be expressed as

$$EOD_u\{C_u^k(t), \vec{\omega}_{bu}\} = \int_0^{T_u} TOP_u\{C_u^k(t), \vec{\omega}_{bu}\} dt. \quad (8)$$

This paper assumes that DUEs move with predefined trajectories $\vec{q}_u(t), \forall u \in \mathcal{U}, t \in [0, T_u]$ and constant velocity V_u , then T_u in (8) can be implied as a fixed parameter posing no impacts on the overall integral. Hence, the EOD of arbitrary DUE u is fully determined by $C_u^k(t)$ and $\vec{\omega}_{bu}$. Without loss of generality, in the following contents of this paper, a specific DUE in Fig. 1 is focused to evaluate our proposed scheme which can be easily applied to other DUEs with orthogonal RB assignment. For enhancing the down-link transmission quality of DUE across its travelling trajectory, this paper focuses on minimizing its EOD. Then, the corresponding optimization problem can be stated as

$$(P1) : \min_{C_u^k(t), \vec{\omega}_{bu}} EOD_u\{C_u^k(t), \vec{\omega}_{bu}\}, \quad (9a)$$

$$\text{s.t.} \sum_{k=1}^K C_u^k(t) \leq 1, \forall t \in [0, T_u], \quad (9b)$$

$$\|\vec{\omega}_{bu}\|^2 = 1, \forall b \in \check{\mathcal{B}}_o^k, \forall t \in [0, T_u], \quad (9c)$$

$$C_u^k(t) \in \{0, 1\}, \forall k \in \mathcal{K}, \forall t \in [0, T_u]. \quad (9d)$$

The constraint (9b) makes sure that the DUE can at most occupy one single RB each time. The constraint (9c) is the normalization requirement for transmit beamforming vector, which ensures

that the transmit power of each available BS $b \in \check{\mathcal{B}}_o^k$ equals to P . The constraint (9d) indicates that $C_u^k(t)$ is a binary variable.

It is extremely challenging to solve the proposed optimization problem (P1), given the listed constraints. The main difficulties can be portrayed as follows: 1) the closed-form expression of $EOD_u\{C_u^k(t), \vec{\omega}_{bu}\}$ should be derived, which is extraordinarily sophisticated, if not impossible; 2) the variations of LoS/NLoS pathloss, small-scale fading \vec{h}_{bu} and the B2G transmit beamforming vector $\vec{\omega}_{bg}$ should be taken into consideration, which are dynamic over time horizon and dependent on their modellings; 3) even given the closed-form expression of the optimization object (9a) and the perfect knowledge of the considered cellular-connected UAV network, it is still mathematically inefficient to be tackled for the non-convexity of mix-integer constraint (9d) and that of the optimization object (9a) w.r.t. $C_u^k(t)$ and $\vec{\omega}_{bu}$. To provide a better alternative solving the proposed optimization problem, DRL-aided solution will be proposed in this paper.

III. THE PROPOSED DRL-AIDED ALGORITHM

In this section, the proposed optimization problem (P1) will be tackled via DRL-based method, i.e., the hybrid D3QN-TD3 algorithm.

A. The Formulation of MDP

To realize the DRL-based solution for the proposed optimization problem (P1), the first step is to formulate (P1) into Markov Decision Process (MDP) which is based on discrete time slots [25]. The length of time slot is defined as δ_u for the considered model and thus the number of time slots equals to $N_u = T_u/\delta_u$ for the DUE u . Note that the duration of time slot δ_u should be picked as small as possible, to achieve that the distances between the DUE and BSs remain approximately constant in each time slot. In this regard, the EOD expression can be rewritten as

$$EOD_u\{C_u^k(n), \vec{\omega}_{bu}\} \approx \sum_{n=1}^{N_u} \delta_u TOP_u\{C_u^k(n), \vec{\omega}_{bu}\}. \quad (10)$$

However, even with given $C_u^k(n)$, the closed-form expression of the transmission outage probability $TOP_u\{C_u^k(n), \vec{\omega}_{bu}\}$ is still difficult to be derived, for its complex formulation and the lack of designed B2U transmit beamforming vector $\vec{\omega}_{bu}$. Alternatively, this challenge can be circumvented via numerical evaluation on the raw measurements of received signals at the DUE. The reason is that, compared to the length of time slot δ_u (typically on the magnitude

of seconds), the length of channel coherence blocks (typically on the magnitude within milliseconds) is relatively small. Then, provided with $C_u^k(n)$ for a time slot n , the indicator of TOP can be defined as $ITOP_u\{C_u^k(n), \vec{\omega}_{bu}(n, i); \hat{h}(n, i)\} = 1$ in the case of $\Gamma_u(n, i) < \Gamma_{th}$, and $ITOP_u\{C_u^k(n), \vec{\omega}_{bu}(n, i); \hat{h}(n, i)\} = 0$ otherwise, where $\hat{h}(n, i)$ and $\vec{\omega}_{bu}(n, i)$ indicate one realization of small-scale fading and that of corresponding beamforming vector, respectively.

Then, the corresponding TOP can be calculated as

$$TOP_u\{C_u^k(n), \vec{\omega}_{bu}\} = \mathbb{E}_{\hat{h}, \vec{\omega}} \left[ITOP_u\{C_u^k(n), \vec{\omega}_{bu}(n, i); \hat{h}(n, i)\} \right]. \quad (11)$$

To realize the average calculation $\mathbb{E}_{\hat{h}, \vec{\omega}}$ over \hat{h} and $\vec{\omega}$ in (11), ς times of SINR measurement should be performed. Furthermore, the arithmetic TOP of the DUE u can be expressed as

$$T\bar{O}P_u\{C_u^k(n), \vec{\omega}_{bu}\} = \frac{1}{\varsigma} \sum_{i=1}^{\varsigma} ITOP_u\{C_u^k(n), \vec{\omega}_{bu}(n, i); \hat{h}(n, i)\}. \quad (12)$$

When sufficiently large amount of SINR measurements is performed, i.e., $\varsigma \gg 1$, the statistical average in (11) can be alternatively replaced by its arithmetic counterpart in (12).⁶ Thereafter, the EOD expression in (10) can be modified as

$$EOD_u\{C_u^k(n), \vec{\omega}_{bu}\} \approx \sum_{n=1}^{N_u} \sum_{i=1}^{\varsigma} \frac{\delta_u}{\varsigma} ITOP_u\{C_u^k(n), \vec{\omega}_{bu}(n, i); \hat{h}(n, i)\}. \quad (13)$$

Then, the original optimization problem (P1) can be approximately revised as

$$(P2) : \min_{C_u^k(n), \vec{\omega}_{bu}(n, i)} \sum_{n=1}^{N_u} \sum_{i=1}^{\varsigma} \frac{\delta_u}{\varsigma} ITOP_u\{C_u^k(n), \vec{\omega}_{bu}(n, i); \hat{h}(n, i)\}, \quad (14a)$$

$$\text{s.t.} \sum_{k=1}^K C_u^k(n) \leq 1, \forall n \in [1, N_u], \quad (14b)$$

$$\|\vec{w}_{bu}(n, i)\|^2 = 1, \forall b \in \check{\mathcal{B}}_o^k, \forall n \in [1, N_u], \quad (14c)$$

$$C_u^k(n) \in \{0, 1\}, \forall k \in \mathcal{K}, \forall n \in [1, N_u]. \quad (14d)$$

In the considered system model, the terrestrial BSs are controlled by a central coordinator (C2) via high-speed broadband cables (e.g., optical fibers), to realize the joint RB allocation and beamforming design task. Once the DUE u registers into the cellular network, the C2 will first check the overall RB availability of all BSs, after which a map of RB possession (RBP) formulated as a 2D matrix $\mathcal{C}(n) = [C_b^k(n)]_{b \times k}$ will be generated. Note that $C_b^k(n) = 1$ if RB k is occupied by BS b at time slot n and $C_b^k(n) = 0$ otherwise. Then, for each RB k , following

⁶In the case of $\varsigma \rightarrow +\infty$, $\lim_{\varsigma \rightarrow +\infty} T\bar{O}P_u\{C_u^k(n), \vec{\omega}_{bu}\} = TOP_u\{C_u^k(n), \vec{\omega}_{bu}\}$ can be guaranteed theoretically.

the RB allocation criterion presented in Subsection II-A, the corresponding occupied set \mathcal{B}_o^k , the potential set $\hat{\mathcal{B}}_o^k$ and the available set $\check{\mathcal{B}}_o^k$ can be determined. Taking the advantage of macro-diversity gain, the C2 will assign all available BSs $b \in \check{\mathcal{B}}_o^k$ to serve the DUE cooperatively. Note that $\mathcal{C}(n)$ remains constant within each time slot and varies among different time slots⁷, capturing the dynamics of RBP at terrestrial BSs. For each time slot, the current location of the DUE $\vec{q}_u(n)$ is observable. Then, the large-scale fading distribution between the DUE and BSs can be traced, via checking the potential blockages between the DUE and each BS according to the local building distribution as mentioned in Subsection II-B. From the point of view on SINR in (6), the allocated RB k serving the DUE can affect the value of SINR in terms of how many desired channels and interfering links are introduced. Hence, the selection of RB resource can inherently impact the EOD performance and should be delicately assigned. Next, with specific RB for each time slot, the beamforming strategy adapting to the time-varying small-scale fading component can further affect the EOD performance.

To handle the aforementioned two-step process, a hybrid D3QN-TD3 algorithm is proposed, in which an outer MDP is formulated for the D3QN agent while an inner MDP is forged for the TD3 agent. Specifically, the D3QN determines which RB should be selected for each time slot and the TD3 outputs the proper beamforming vector for each link between the DUE and BSs in the available BS set. Furthermore, the considered cellular-connected UAV network is divided into the outer environment and the inner environment. For time slot n , the DUE's location $\vec{q}_u(n)$ and the RBP map $\mathcal{C}(n)$ can be observed from the outer environment. The inner environment is defined to reflect the time-varying characteristic of small-scale fading, which is dependent on the outer environment. The reason roots from that the B2U channel's small-scale fading component is subject to the corresponding experienced type of pathloss in practice, i.e., LoS or NLoS.

B. Description of the Hybrid D3QN-TD3 Solution

To derive a flexible solution which can solve the proposed optimization problem (P2) in a dynamic RBP and time-varying small-scale fading scenario, both the D3QN and the TD3 networks in the proposed hybrid D3QN-TD3 algorithm are trained interactively. Specifically, the D3QN network maps the outer state and the RB selection into Q-values, while the actor of

⁷To avoid frequent handover, the selected RB k is considered as unchanged within each time slot.

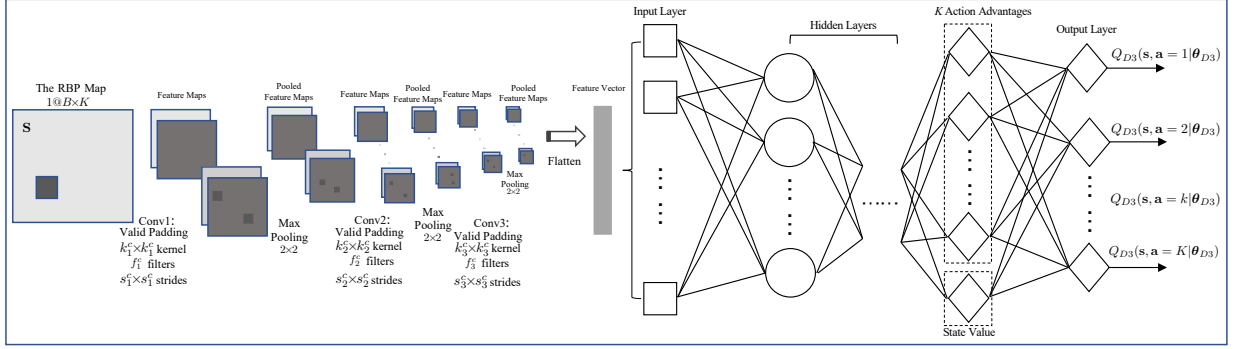


Figure 3: Architecture of CNN-attached duelling DQN

TD3 agent transforms the inner state into beamforming vector and the critic of TD3 network evaluates the corresponding Q values.

1) *D3QN*: To tackle the RB allocation problem, state-of-the-art DQN with duelling architecture will be invoked to approximate Q function for the outer MDP. Compared to the original DQN method, the duelling DQN explicitly separates the representation of state value and the corresponding action advantages into two independent streams, as depicted in Fig. 3. Specifically, the duelling DQN first estimates the state value and the action advantages that are dependent on the state, and then calculates Q value for each state-action pair via aggregation. The duelling architecture can help approximate Q function more robustly and efficiently, especially when the Q values of various actions with the same state are indistinguishable.

The outer MDP for the D3QN agent can be formulated as follows. The outer state s is the observed RBP map $\mathcal{C}(n)$ ⁸, while the outer action a refers to the selected RB $k^* = \arg\{C_u^k(n) = 1\}$. When the dimensionality of $\mathcal{C}(n)$ is large, the computation and training burdens could be unbearable if the RBP map is just flattened and then fed to the input layer of D3QN. To circumvent this issue, a convolutional neural network (CNN) is attached to the D3QN, for efficiently capturing the features of the RBP map and compressing the data fed into the D3QN. Specifically, the CNN contains three convolutional layers, i.e., Conv1, Conv2 and Conv3, as depicted in Fig. 3 where the corresponding size of kernel, amount of filter and size of stride are denoted. Following each convolutional layer, a standard max pooling layer with pool size 2×2 and stride 2×2 is invoked. At the end, the pooled feature maps will be flattened into a vector which will then be fed into the input layer of D3QN. The considered optimization problem is

⁸The transition of RBP map is stochastic and can be observed from the outer environment, which means that the D3QN learning process is model-free.

fully determined by the value of SINR, given SINR threshold. In other word, larger available BS set and smaller occupied BS set are favourable to minimize the EOD. For outer state s and the selected outer action a , the corresponding available BS set $\check{\mathcal{B}}_o^{k^*}$ and the occupied BS set $\mathcal{B}_o^{k^*}$ can be determined according to Subsection II-A. Then, the outer reward function is defined as

$$\mathbf{r} = \frac{\text{card}(\check{\mathcal{B}}_o^{k^*})}{\text{card}(\check{\mathcal{B}}_o^{k^*}) + \text{card}(\mathcal{B}_o^{k^*})}. \quad (15)$$

The designed outer reward function (15) infers that the selected RB k^* resulting in larger available BS set and smaller occupied BS set is more favourable. Given the formulation of outer MDP, the duelling DQN is invoked to approximate $Q_{D3}(s, a|\boldsymbol{\theta}_{D3})$ where $\boldsymbol{\theta}_{D3}$ represents the parameter vector of D3QN network. The D3QN network is trained to minimize its loss function via the gradient descent updating rule, shown as

$$\boldsymbol{\theta}_{D3}(t+1) = \boldsymbol{\theta}_{D3}(t) - \alpha_{D3} \nabla_{\boldsymbol{\theta}_{D3}} \text{loss}(\boldsymbol{\theta}_{D3}), \quad (16)$$

where α_{D3} denotes the learning rate and $\nabla_{\boldsymbol{\theta}_{D3}} \text{loss}(\boldsymbol{\theta}_{D3})$ represents the gradient of the D3QN network's loss function w.r.t. $\boldsymbol{\theta}_{D3}$. For a mini-batch of N_{D3} transitions randomly sampled from the outer replay buffer, the mean-square loss function in (16) is defined as

$$\text{loss}(\boldsymbol{\theta}_{D3}) = \frac{1}{N_{D3}} \sum_{t=1}^{N_{D3}} [y_t - Q_{D3}(s_t, \mathbf{a}_t|\boldsymbol{\theta}_{D3})]^2, \quad (17)$$

where $y_t = \mathbf{r}_t + \gamma Q_{D3}(s_{t+1}, \mathbf{a}_{t+1}^*|\boldsymbol{\theta}_{D3}^-)$ and $\boldsymbol{\theta}_{D3}^-$ indicates the parameter vector of target D3QN network. Note that the optimal outer action for the next outer state s_{t+1} is selected by the D3QN network instead of the target D3QN network, given by

$$\mathbf{a}_{t+1}^* = \arg \max_{\mathbf{a}_{t+1}} Q_{D3}(s_{t+1}, \mathbf{a}_{t+1}|\boldsymbol{\theta}_{D3}). \quad (18)$$

In this manner, the bootstrapping outer action is evaluated by the target D3QN network while the selection of outer action is achieved by the D3QN network, completing the double Q learning procedure. Applying double Q learning method to separate action selection and bootstrapping evaluation into two networks can help address the overestimation bias issue introduced by the max operator in calculating the loss function. After several steps of updating the D3QN network, the target D3QN network will be synchronized to the D3QN network via letting $\boldsymbol{\theta}_{D3}^- = \boldsymbol{\theta}_{D3}$.

Given outer state s , the outer action selection strategy applied by the D3QN agent follows the popular ϵ -greedy policy, shown as

$$\mathbf{a} = \begin{cases} \text{randi}(K), & \text{with probability } \epsilon \\ \arg \max_{k=1, \dots, K} Q_{D3}(s, k|\boldsymbol{\theta}_{D3}), & \text{otherwise} \end{cases}, \quad (19)$$

where the exploration parameter $\epsilon \in [0, 1]$ is used to balance exploration and exploitation in learning process. Specifically, larger ϵ encourages the D3QN agent to explore the outer action space, while smaller ϵ results in more frequent exploitation of learned knowledge. Usually, the exploration parameter ϵ is annealing alongside the learning process, steering the D3QN agent from more frequent exploration to higher probability of exploitation.

2) *TD3*: For each time slot n , the D3QN agent observes the outer environment, from which it obtains the DUE's location $\vec{q}_u(n)$ and the RBP map $\mathcal{C}(n)$. Then, the D3QN agent selects the outer action, i.e., the RB k^* . With the selected RB and the current RBP map, the corresponding set of available BSs $\check{\mathcal{B}}_o^{k^*}$ can be determined. To reduce the overheads of CSI estimation and inner reward feedback, a random BS out of the current available BSs will be selected by the C2 to perform beamforming optimization. Thereafter, the type of large-scale fading between the DUE and the chosen available BS can be obtained. Then, the inner MDP for the TD3 network can be formulated as follows. Each inner state \hat{s} consists of a list of estimated CSI $\vec{h}_{bu}(n, i)$ and its corresponding type of LoS or NLoS. It is well known that ANNs only accept real numbers as their inputs, rather than complex values. To circumvent this problem, the complex-value estimated CSI $\vec{h}_{bu}(n, i)$ will be transferred into a flatten layer which decouples the complex value and reshapes its real and imagery parts into a real-value vector. However, the inner state \hat{s} is dominated by the flattened CSI, while only one dimension is left for the indicator of pathloss type, which raises the issue of dimension imbalance. To solve this, the dimension for pathloss type indicator will be expanded from 1 to M via duplicating the pathloss type indicator into M copies, making it comparable to the dimension of flattened CSI. Each possible inner action \hat{a} generated from the actor network is a vector of real-value numbers, which will be reshaped into a normalized complex-value vector to construct the corresponding beamforming vector $\vec{w}_{bu}(n, i)$. The transitions of inner states are determined by the experienced small-scale fading model. The inner reward function evaluates how good the selected inner action is for each time of state transition. To reflect the quality of selected inner action, the inner reward function is defined as

$$\hat{r} = \frac{|\vec{h}_{bu}(n, i)\vec{w}_{bu}(n, i)|^2}{\|\vec{h}_{bu}(n, i)\|^2}. \quad (20)$$

TD3 method belongs to actor-critic algorithms, in which the critic network learns Q function approximation $Q_P(\hat{s}, \hat{a}|\theta_P)$ and the actor network is the policy generator approximating the action $\mu(\hat{s}|\theta_\mu)$, where θ_P and θ_μ denote the parameter vectors of critic and actor networks, respectively. Specifically, the actor network takes the inner state as its input and generates deter-

ministic continuous action as its output, unlike DQN-related methods that output a probability distribution over discrete action space. Furthermore, the inner action generated by the actor network will be leveraged to the input layer of the critic network together with the current inner state. Then, the corresponding state-action value will be generated at the output layer of the critic network. The actor network is invoked to approximate the inner action and thus the exhaustive search of the optimal inner action maximizing the Q function given the next inner state is avoided. Fig. 4 depicts the overall architecture of TD3 network.

The gradient descent updating on the twin critic networks can be given by

$$\boldsymbol{\theta}_{P_j}(t+1) = \boldsymbol{\theta}_{P_j}(t) - \alpha_{P_c} \nabla_{\boldsymbol{\theta}_{P_j}} \text{loss}(\boldsymbol{\theta}_{P_j}), \quad (21)$$

where α_{P_c} indicates the learning rate, $\nabla_{\boldsymbol{\theta}_{P_j}} \text{loss}(\boldsymbol{\theta}_{P_j})$ denotes the gradient of critic network's loss function w.r.t. $\boldsymbol{\theta}_{P_j}$ and $\hat{j} \in \{1, 2\}$ is defined to distinguish the twin critics. Besides, the corresponding mean-square loss function is defined as

$$\text{loss}(\boldsymbol{\theta}_{P_j}) = \frac{1}{N_P} \sum_{t=1}^{N_P} \left[\hat{y}_t - Q_P(\hat{\mathbf{s}}_t, \hat{\mathbf{a}}_t | \boldsymbol{\theta}_{P_j}) \right]^2, \quad (22)$$

where

$$\hat{y}_t = \hat{\mathbf{r}}_t + \gamma \min_{\hat{j}=1,2} Q_P[\hat{\mathbf{s}}_{t+1}, \mu(\hat{\mathbf{s}}_{t+1} | \boldsymbol{\theta}_{\mu}^-) + \mathcal{N}^- | \boldsymbol{\theta}_{P_j}^-] \quad (23)$$

represents the target Q value, N_P is from a mini-batch of N_P transitions extracted from the inner replay buffer, and $\boldsymbol{\theta}_{P_j}^-$, $\boldsymbol{\theta}_{\mu}^-$ and \mathcal{N}^- denote the parameters of target critic network, those of target actor network and additive noise for target actor network, respectively. Note that the operator min in (23) and \mathcal{N}^- are posed for accomplishing clipped double Q learning and target policy smoothing, respectively.

Moreover, the actor network aims to maximize its expected return, defined as

$$J(\boldsymbol{\theta}) = \mathbb{E}_{\hat{\mathbf{s}}_t} \{ Q[\hat{\mathbf{s}}_t, \mu(\hat{\mathbf{s}}_t | \boldsymbol{\theta}_{\mu}) | \boldsymbol{\theta}_P] \}, \quad (24)$$

of which the derivative w.r.t. $\boldsymbol{\theta}_{\mu}$ can be calculated with help of the chain rule, shown as

$$\begin{aligned} \nabla_{\boldsymbol{\theta}_{\mu}} J(\boldsymbol{\theta}) &\approx \mathbb{E}_{\hat{\mathbf{s}}_t} \{ \nabla_{\boldsymbol{\theta}_{\mu}} Q[\hat{\mathbf{s}}_t, \mu(\hat{\mathbf{s}}_t | \boldsymbol{\theta}_{\mu}) | \boldsymbol{\theta}_P] \} \\ &= \frac{1}{N_P} \sum_{t=1}^{N_P} \nabla_a Q_P(\hat{\mathbf{s}}_t, a | \boldsymbol{\theta}_{P_1}) \nabla_{\boldsymbol{\theta}_{\mu}} \mu(\hat{\mathbf{s}}_t | \boldsymbol{\theta}_{\mu}), \end{aligned} \quad (25)$$

in which the critic 1 is anchored by the chain rule for simplicity.

Then, the gradient ascent updating of the actor network can be expressed as

$$\boldsymbol{\theta}_{\mu}(t+1) = \boldsymbol{\theta}_{\mu}(t) + \alpha_{P_a} \nabla_{\boldsymbol{\theta}_{\mu}} J(\boldsymbol{\theta}), \quad (26)$$

where α_{Pa} is the learning rate of the actor network. Moreover, to complete the delayed policy update procedure, the actor, target actor and the twin target critics will be updated less frequently than the twin critics, via updating the target networks every N_{pud} times the twin critics are trained.

Furthermore, the Polyak averaging updates for the target critic and actor networks are applied to enhance the stability of learning, given by

$$\theta_{P_j}^- \leftarrow \tau \theta_{P_j} + (1 - \tau) \theta_{P_j}^-, \quad (27)$$

$$\theta_{\mu}^- \leftarrow \tau \theta_{\mu} + (1 - \tau) \theta_{\mu}^-, \quad (28)$$

respectively, where τ is the interpolation factor in Polyak averaging method for updating target networks and it is usually set to be close to zero, i.e., $\tau \ll 1$.

Different from probabilistic action selection policy on discrete actions for D3QN agent, exploration on continuous actions for TD3 agent can be realized via adding noise sampled from a noise process \mathcal{N} to the actor network, i.e., $\hat{\mathbf{a}} \leftarrow \hat{\mathbf{a}} + \mathcal{N}$, where \mathcal{N} can be chosen to adapt to the inner environment [26]. For simplicity, zero-mean Normal noise with variance σ_P^2 is applied to generate artificial noise for the output of actor network, where σ_P^2 is annealing alongside the learning process to guide the TD3 agent from exploration to exploitation. Without loss of generality, the additive noise posed on the target actor network \mathcal{N}^- is generated from zero-mean Normal distribution with annealing variance σ_P^2 as well.

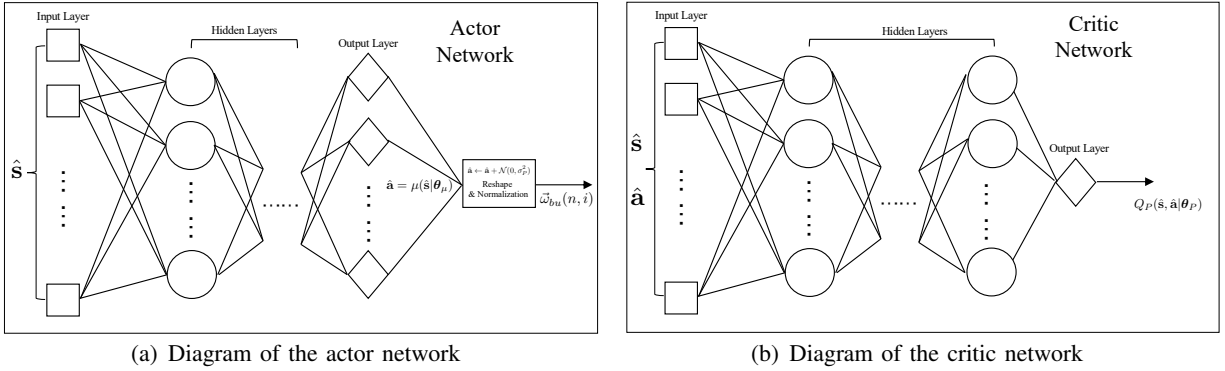


Figure 4: Architecture of TD3 network

3) *The Hybrid D3QN-TD3 Algorithm:* The overall pseudo-code and interacting diagram of the proposed hybrid D3QN-TD3 solution are given by **Algorithm 1** and Fig. 5, respectively. All the neural networks as well as their corresponding target networks and replay buffers are first initialized (line 1). For each learning episode, the outer environment will be initialized, which means that the drone's location should be reset to the start coordinate of the given trajectory

and the RBP map should be re-observed as well (line 3 and 5). For each outer epoch in a learning episode, the D3QN agent picks the outer action \mathbf{a}_i according to the ϵ -greedy action selection policy (19) and then the corresponding available set $\check{\mathcal{B}}_o^{\mathbf{a}_i}$ and the occupied set $\mathcal{B}_o^{\mathbf{a}_i}$ can be determined following the RB allocation regulation as mentioned in Subsection II-A (line 6). Based on the local building distribution as introduced in Subsection II-B, the types of wireless links (LoS or NLoS) between the DUE and BSs in the available set $\check{\mathcal{B}}_o^{\mathbf{a}_i}$ can be determined. To initialize the inner environment for each outer epoch, a random available BS will be selected from set $\check{\mathcal{B}}_o^{\mathbf{a}_i}$ (line 7). Furthermore, the actor of TD3 agent selects the inner action $\hat{\mathbf{a}}_j$. After executing the noised inner action, the TD3 agent can observe the next inner state $\hat{\mathbf{s}}_{j+1}$ from the inner environment and then calculate the immediate reward $\hat{\mathbf{r}}_j$ (line 10). Transitions of the inner MDP will be stored into the inner replay buffer, i.e., $(\hat{\mathbf{s}}_j, \hat{\mathbf{a}}_j, \hat{\mathbf{s}}_{j+1}, \hat{\mathbf{r}}_j) \rightarrow \hat{\mathbf{R}}$ (Line 11). After at least N_P times of interaction between the TD3 agent and the inner environment, a mini-batch of N_P transitions will be sampled from $\hat{\mathbf{R}}$ to train the twin critics, via gradient descent method in (21) (line 12). For every N_{pud} times of training the twin critic networks, the actor network will be trained as per gradient ascent approach in (26), and the target twin critic and the target actor networks will be updated following Polyak averaging rule (line 13). After the evaluation and training of the TD3 agent, the selected outer action \mathbf{a}_i will be conducted and the next outer state \mathbf{s}_{i+1} can be observed from the outer environment, then the immediate outer reward \mathbf{r}_i can be derived (line 15). Furthermore, transitions of the outer MDP will be stored into the outer replay buffer \mathbf{R} , i.e., $(\mathbf{s}_i, \mathbf{a}_i, \mathbf{s}_{i+1}, \mathbf{r}_i) \rightarrow \mathbf{R}$ (line 16). When at least N_{D3} transitions are recorded into \mathbf{R} , a mini-batch of N_{D3} transitions will be randomly sampled from \mathbf{R} , which will be utilized to train the online D3QN network (line 17). For every Υ_{D3} steps, the target D3QN network will be updated to the online D3QN network via letting $\boldsymbol{\theta}_{D3}^- = \boldsymbol{\theta}_{D3}$ (line 18). For each training episode, the exploration parameter ϵ and Normal noise variance σ_P^2 will be annealed by their respective decaying rates to deal with the dilemma of exploration and exploitation (line 20).

IV. SIMULATION RESULTS

In this section, numerical results will be provided to evaluate the performance of the proposed hybrid D3QN-TD3 solution. An urban subregion specified by $[0, 3] \times [0, 3] \times [0, 0.1]$ (in km) is focused, in which local building distribution is generated via one realization of ITU statistical model as shown in Fig. 2. The parameter setting of this statistical model is in line with those in Subsection II-B2. Note that the generated building distribution remains stable and unchanged

Algorithm 1: The proposed hybrid D3QN-TD3 solution

```

1 Initialization: Initialize randomly the D3QN network  $Q_{D3}(s, a|\theta_{D3})$  and its target network  $Q_{D3}(s, a|\theta_{D3}^-)$ , with  $\theta_{D3}^- \leftarrow \theta_{D3}$ . Initialize randomly the TD3 network, including the actor network  $\mu(s|\theta_\mu)$ , the twin critic networks  $Q_P(s, a|\theta_{P_j})$ , the target actor network  $\mu(s|\theta_\mu^-)$  and the twin target critic networks  $Q_P(s, a|\theta_{P_j}^-)$ , with  $\theta_\mu^- \leftarrow \theta_\mu$  and  $\theta_{P_j}^- \leftarrow \theta_{P_j}$ . Initialize the D3QN replay buffer  $\hat{R}$  with capacity  $\hat{D}$  and the TD3 replay buffer  $\hat{R}$  with capacity  $\hat{D}$ ;
2 for  $episode = [1, ep_i]$  do
3   Initialize the outer environment and reset the UAV's location to  $\bar{q}_u(0)$ ;
4   for  $i = [1, ep_{outer}]$  do
5     Observe the outer state  $s_i$ ;
6     Select the outer action  $a_i$ , observe the available set  $\tilde{\mathcal{B}}_o^{a_i}$  and the occupied set  $\mathcal{B}_o^{a_i}$ ;
7     Randomly select a BS  $\tilde{b} \in \tilde{\mathcal{B}}_o^{a_i}$  and check the corresponding type of pathloss, i.e., LoS or NLoS, then initialize the inner environment;
8     for  $j = [1, ep_{inner}]$  do
9       Observe the inner state  $\hat{s}_j$ ;
10      Select and execute the inner action  $\hat{a}_j$ , then observe the next inner state  $\hat{s}_{j+1}$  and calculate the corresponding inner reward  $\hat{r}_j$ ;
11      Store transition  $(\hat{s}_j, \hat{a}_j, \hat{s}_{j+1}, \hat{r}_j)$  into  $\hat{R}$ ;
12      Sample a mini-batch of  $N_P$  transitions from  $\hat{R}$ , then update the twin critic networks  $Q_P(s, a|\theta_{P_j})$  via gradient descent method in (21);
13      Every  $N_{Pud}$  times the twin critics are trained, update the actor network  $\mu(s|\theta_\mu)$  via gradient ascent approach in (26), and update the target networks  $Q_P(s, a|\theta_{P_j}^-)$  and  $\mu(s|\theta_\mu^-)$ , following the Polyak averaging rule in (27) and (28), respectively;
14    end
15    Execute the outer action  $a_i$ , then observe the next outer state  $s_{i+1}$  and calculate the outer reward  $r_i$ ;
16    Store transition  $(s_i, a_i, s_{i+1}, r_i)$  into  $R$ ;
17    Sample a mini-batch of  $N_{D3}$  transitions from  $R$ , then update the D3QN network  $Q_{D3}(s, a|\theta_{D3})$  via gradient descent method in (16);
18    Update the D3QN target network  $Q_{D3}(s, a|\theta_{D3}^-)$  every  $\Upsilon_{D3}$  steps, i.e.,  $\theta_{D3}^- \leftarrow \theta_{D3}$ ;
19  end
20  Update  $\epsilon \leftarrow \epsilon \times dec_\epsilon$  and  $\sigma_P^2 \leftarrow \sigma_P^2 \times dec_\sigma$ ;
21 end

```

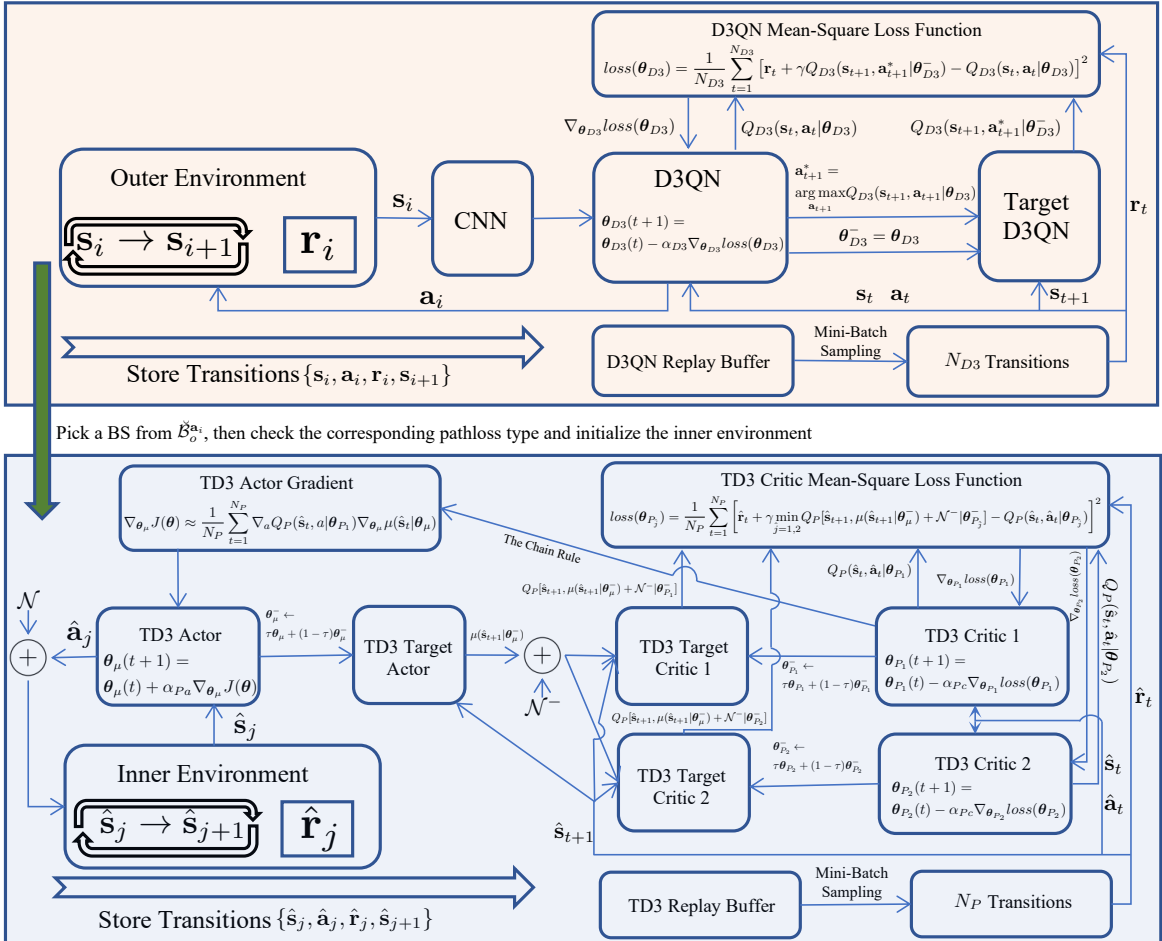


Figure 5: Workflow of the hybrid D3QN-TD3 solution

for the entire simulation process, which consents with the practical scenario in real life. In our considered model, the DUE's location at each time slot is observed to determine the LoS/NLoS links via checking potential blockages between the DUE and the BSs.

For ease of implementation, the DUE's initial location and destination are fixed at $\vec{q}_u(I) = (1, 1, 0.1)$ km and $\vec{q}_u(D) = (2, 2, 0.1)$ km, respectively. The given trajectory is defined as the line between $\vec{q}_u(I)$ and $\vec{q}_u(D)$, of which the length is $\sqrt{\|\vec{q}_u(D) - \vec{q}_u(I)\|^2} \approx 1.4$ km. Besides, the velocity of DUE is set as $V_u = 35$ m/s and hence the DUE will spend $T_u = 40$ s to travel between $\vec{q}_u(I)$ and $\vec{q}_u(D)$. Nakagami- m fading⁹ is taken as an example to model the small-scale fading component for B2U channels in this paper. The shape factor m in Nakagami- m fading is assumed as 3 for LoS and 1 for NLoS. For the correlation coefficient in the imperfect B2U CSI model (5), we set $\rho = 0.75$. Besides, we apply the popularly-used Rayleigh fading [27] to model the terrestrial small-scale fading component and the beamforming vector for terrestrial transmission is set as $\vec{w}_{bg} = \vec{h}_{bg}^\dagger / \|\vec{h}_{bg}\|$ for simplicity.¹⁰ Unless otherwise mentioned, the simulation parameter settings are in accordance with Table I.

A. Construction of DNNs

The proposed hybrid D3QN-TD3 solution is implemented on Python 3.8 with TensorFlow 2.3.1 and Keras. The optimizer minimizing the mean-square error (MSE) for all the applied deep neural networks (DNNs) is *Adam* with fixed learning rate. The activation function at each hidden layer (including each convolutional layer of CNN) is *Relu* function, for its simplicity and generality. Besides, the activation function utilized for both output layers in D3QN and critic network of TD3 is *Linear*, while that for actor network of TD3 is *Tanh*.

The DNN of D3QN agent is constructed with fully connected feedforward artificial neural network (ANN), in which 3 hidden layers contain 512, 256 and 128 neurons, respectively. The shapes of CNN's input and output layer of D3QN are determined by the dimension of RBP map

⁹In contrast to terrestrial communication scenarios where Rayleigh fading is widely applied to model small-scale fading, Rician or Nakagami- m fading is more suitable to track the characteristics of B2U small-scale fading when LoS pathloss is experienced. For Nakagami- m fading model, special case $m = 1$ is equivalent to Rayleigh fading while the case with $m > 1$ can be utilized as an alternative of Rician fading where m reflects the strength of LoS component.

¹⁰This paper focuses on the interference management for cellular-connected UAV networks and the precoding configuration regarding terrestrial transmissions is not our interest. Here, we assume that the occupied BSs simply perform MRT technique for their serving GUEs.

Table I: Simulation parameter settings

Parameters	Values	Parameters	Values
Capacities of replay buffers $\mathring{D}/\mathring{D}$	100,000/100,000	Given TOP threshold Γ_{th}	0 dB
Number of episodes epi	100	Capacity of \mathcal{B}	37
Number of outer epochs epo_{outer}	22	Capacity of \mathcal{K}	100
Number of inner epochs epo_{inner}	200	Transmit power of each BS P	15 dBm
Target network update frequency Υ_{D3}	500	Number of antennas at each BS M	8
Initial exploration parameter ϵ/σ_P^2	0.9/1	Tier of ICI p	1
Exploration annealing rate dec_e/dec_σ	0.93/0.91	Power of AWGN σ^2	-90 dBm
Size of mini-batch N_{D3}/N_P	128/128	Carrier frequency f_c	2 GHz
Polyak interpolation factor τ	0.00005	DUE's Altitude h /BS's antenna height z	100 m/25 m
Learning rates $\alpha_{D3}/\alpha_{Pc}/\alpha_{Pa}$	0.001/0.002/0.001	SINR measurements ς	1000
Discount factor γ	0.99	Duration of time slot δ_u	1.82 s
Nakagami shape factor m for LoS/NLoS	3/1	Imperfect B2D CSI correlation factor ρ	0.75
Policy update delay factor N_{pud}	2	Prior-activation penalty coefficient κ	1
Absolute saturation value of Tanh ξ	2.5	Size of CNN's kernel $k_1^c/k_2^c/k_3^c$	5/4/3
Number of CNN's filter $f_1^c/f_2^c/f_3^c$	32/32/32	Size of CNN's stride $s_1^c/s_2^c/s_3^c$	1/1/1

and the number of possible RBs, i.e., $card(\mathcal{B}) \times card(\mathcal{K})$ and $card(\mathcal{K})$, respectively. Before the output layer and after the last hidden layer, there is a duelling layer with $card(\mathcal{K}) + 1$ neurons, where one neuron reflects the estimation of state-value and the remaining $card(\mathcal{K})$ neurons track the action advantages for the $card(\mathcal{K})$ possible actions. After aggregation, the output layer generates the estimation of the $card(\mathcal{K})$ state-action values, as depicted in Fig. 3.

Both the twin critic and actor networks' DNNs in TD3 agent are fully connected feedforward ANNs with 3 hidden layers consisting of 512, 256 and 128 neurons. The dimensions of input layer and output layer of the twin critic networks correspond to $2M + M + 2M$ and 1, while those of the actor network are $2M + M$ and $2M$, respectively. This is because the Nakagami- m fading component is in form of complex value, which should be decoupled at the input layers of the critic and actor networks. Besides, M additional neurons should be added into the input layers of the critic and actor networks to help them identify LoS/NLoS inner environment. To calculate the inner reward function (20), the actor network's outputs will be reconstructed into complex-value vector with $M \times 1$ dimension, after which the vector will be normalized to satisfy constraint (14c).

Although activation function $Tanh$ is popular and effective, it may suffer from saturation. As depicted in Fig. 6, when the input of $Tanh$ locates in the left (right) saturation region, the corresponding output will unreasonably approach -1 (1), raising gradient vanishing issue amid

back-propagation of the training process. To tackle this problem, prior-activation penalty will be posed onto the actor network's loss function, which can direct the input of *Tanh* to remain in the range of unsaturation area. In implementation, gradient ascent on actor's expected return (26) is accomplished via inverse batch gradient descent on the estimated Q function of critic 1 network, given by

$$\boldsymbol{\theta}_\mu(t+1) = \boldsymbol{\theta}_\mu(t) - \alpha_{Pa} \nabla_{\boldsymbol{\theta}_\mu} \text{loss}(\boldsymbol{\theta}_\mu), \quad (29)$$

where the mean loss function of actor network is denoted as

$$\text{loss}(\boldsymbol{\theta}_\mu) = -\frac{1}{N_P} \sum_{t=1}^{N_P} Q_P[\hat{\mathbf{s}}_t, \mu(\hat{\mathbf{s}}_t | \boldsymbol{\theta}_\mu) | \boldsymbol{\theta}_{P_1}]. \quad (30)$$

Then, to perform prior-activation penalty trick, the mean loss function of actor network (30) is rewritten as

$$\begin{aligned} \text{loss}(\boldsymbol{\theta}_\mu) = & \frac{1}{N_P} \sum_{t=1}^{N_P} \left\{ -Q_P[\hat{\mathbf{s}}_t, \mu(\hat{\mathbf{s}}_t | \boldsymbol{\theta}_\mu) | \boldsymbol{\theta}_{P_1}] + \right. \\ & \left. \kappa \left[\max \left(\frac{1}{2M} \sum_{m=1}^{2M} \varrho_{t,m} - \xi, 0 \right) + \max \left(-\frac{1}{2M} \sum_{m=1}^{2M} \varrho_{t,m} - \xi, 0 \right) \right]^2 \right\}, \quad (31) \end{aligned}$$

where κ indicates the coefficient of prior-activation penalty, ξ represents the absolute saturation value of *Tanh* activation function, and $\varrho_{t,m}$ denotes the prior-activation value of the corresponding neuron $m = \{1, 2, \dots, 2M\}$ over one time of sampling t from mini-batch transitions. The actor is trained to minimize (31), which can directly navigate the prior-activation values of actor's output neurons to remain in the unsaturation region and thus helping circumvent the issue of gradient vanishing caused by saturation.

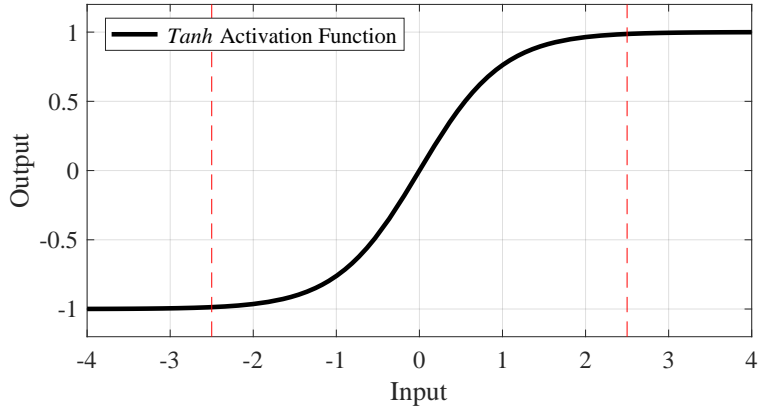


Figure 6: An illustration on saturation of Tanh activation function

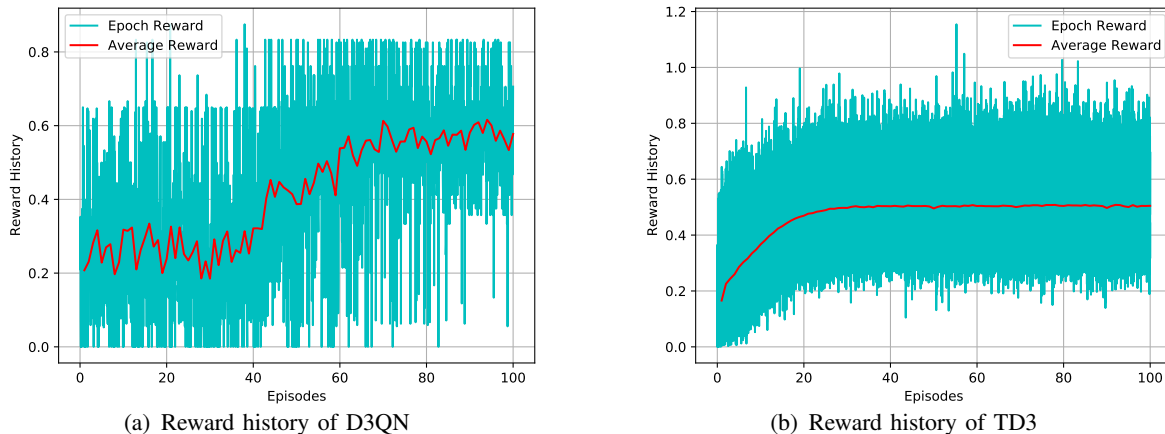


Figure 7: Reward history

B. Training of Hybrid D3QN-TD3 Algorithm

Fig. 7 shows reward history curves versus training episodes for the proposed hybrid D3QN-TD3 solution. The average reward reflects the expected value of epoch rewards for each episode, which is calculated via averaging accumulated rewards over training epochs. It can be observed from Fig. 7 that both D3QN and TD3 networks illustrate increasing trending of average reward alongside the training process, though experiencing some fluctuations that are usual phenomena in the regime of DRL-related algorithms. Specifically, the D3QN’s average reward converges to the optimum (around 0.57) after 70 training episodes, while the TD3 converges to its highest average reward (about 0.51) after 40 training episodes. Fig. 7(a) validates that the D3QN agent can adapt to the dynamic RBP environment via allocating proper RB index to the DUE for each time slot, while Fig. 7(b) verifies that the TD3 agent is able to adjust transmit beamforming vectors to fit the small-scale fading environment. After saving the hybrid D3QN-TD3 model with the highest average rewards, it can be re-loaded to realize EOD performance comparison which will be illustrated in Subsection IV-D.

C. Impacts of Hyper-parameters

It is well known that the overall performance of DRL-related algorithms is sensitive to hyper-parameters, e.g., target network update and learning rate. The hyper-parameters should be picked carefully for given system settings, to realize satisfactory learning quality and convergence speed.

Fig. 8(a) delivers average D3QN reward curves versus training episodes with various α_{D3} , while Fig. 9(a) demonstrates average TD3 reward curves versus training episodes with different combinations of α_{Pa} and α_{Pc} . From these figures, it can be observed that learning rates

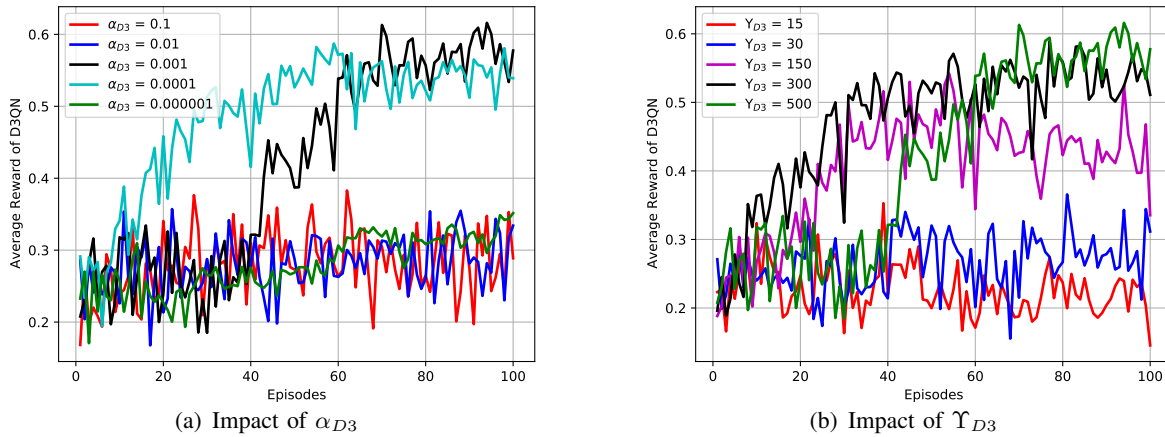


Figure 8: Impact of learning rates and target network update frequency

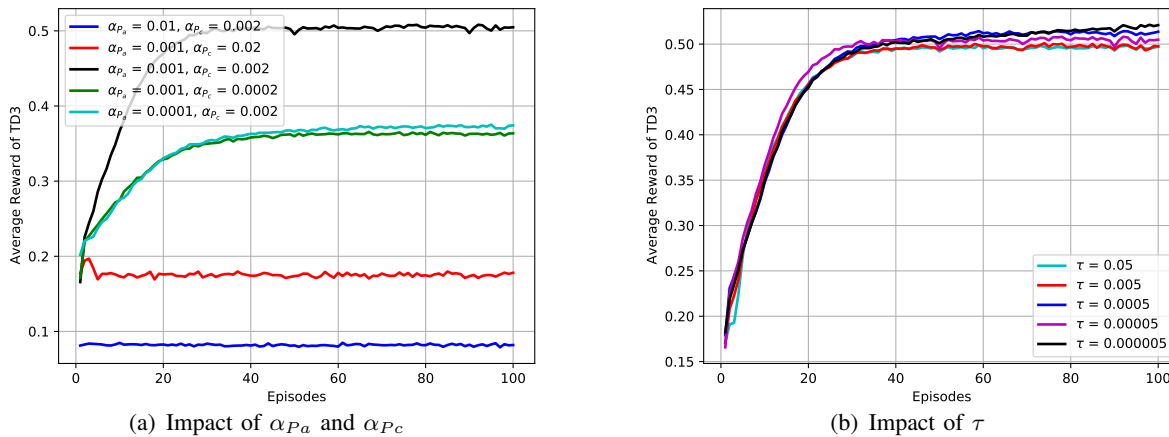


Figure 9: Impact of learning rates and Polyak interpolation factor

pose significant impacts on learning performance and convergence speed. With relatively high α_{D3} , i.e., $\alpha_{D3} = \{0.1, 0.01\}$, although the D3QN’s convergences are quite rapid, it reaches extremely unsatisfactory learning scores (both around 0.3). With relatively small α_{D3} , i.e., $\alpha_{D3} = \{0.001, 0.0001\}$, the D3QN agent can achieve higher scores (about 0.57 and 0.54, respectively). Surprisingly, when α_{D3} is extremely small, i.e., $\alpha_{D3} = 0.000001$, it leads to unsatisfactory learning performance in the range of 100 training episodes. However, $\alpha_{D3} = 0.000001$ may have the potential to help the D3QN agent reach a new highest score, for which the price is that much more training episodes are needed (i.e., less favourable convergence rate). For Fig. 9(a), learning rate combination $[\alpha_{Pa} = 0.001, \alpha_{Pc} = 0.002]$ is selected as the anchor for comparison, which can converge to its optimal score (around 0.51) after about 40 training episodes. With higher α_{Pa} , i.e., $[\alpha_{Pa} = 0.01, \alpha_{Pc} = 0.002]$, the TD3 agent barely learns anything and achieves significantly worse score (around 0.06). With smaller α_{Pa} , i.e., $[\alpha_{Pa} = 0.0001, \alpha_{Pc} = 0.002]$, the TD3 agent converges to a worse score (about 0.38) than the anchor, after around 60 training episodes, which means that it experiences slower convergence

rate. With higher α_{P_c} , i.e., $[\alpha_{P_a} = 0.001, \alpha_{P_c} = 0.02]$, the TD3 agent converges to worse learning quality (around 0.18), although the corresponding convergence speed is relatively rapid. With smaller α_{P_c} , i.e., $[\alpha_{P_a} = 0.001, \alpha_{P_c} = 0.0002]$, the TD3 agent can only reach much lower learning score (around 0.37), while experiencing a comparable convergence speed (converging after around 40 training episodes). From the above observations, it is straightforward to conclude that the proposed hybrid D3QN-TD3 solution is unsurprisingly sensitive to learning rate which should be selected delicately for accomplishing a good trade-off between learning quality and convergence speed.

Fig. 8(b) depicts average D3QN reward curves versus training episodes with different Υ_{D3} , while Fig. 9(b) illustrates average TD3 reward curves versus training episodes with various τ . From these figures, it can be easily concluded that target network technique adopted in the proposed hybrid D3QN-TD3 algorithm is undoubtedly of essence. Specifically, less frequent updating (i.e., larger Υ_{D3}) on D3QN's target network can help the D3QN agent achieve better learning scores, while less amount of updating (i.e., smaller τ) on TD3's target networks is more favourable. However, larger Υ_{D3} and smaller τ may result in slower convergence speed. Hence, the picking of Υ_{D3} and τ is important for the proposed hybrid D3QN-TD3 solution to deal with the dilemma between learning performance and convergence speed.

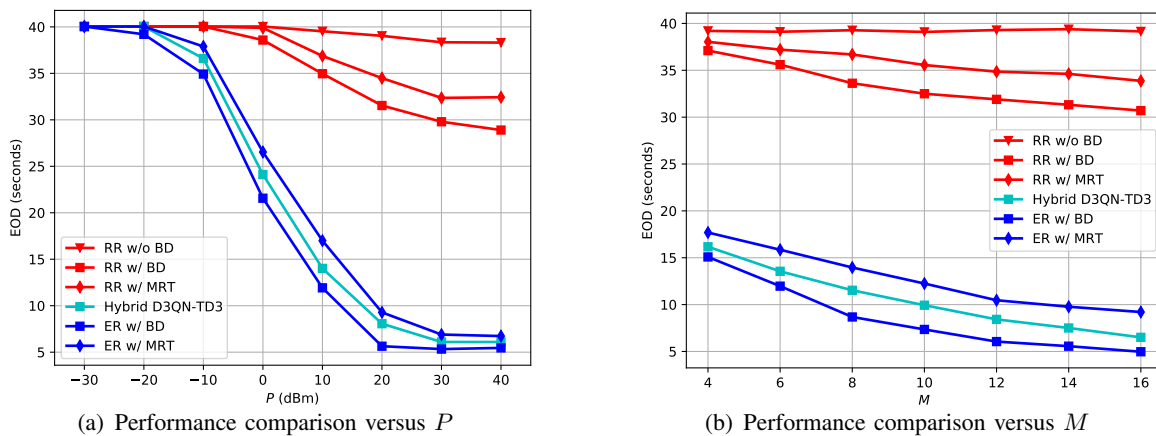


Figure 10: Performance comparison

D. Performance Comparison

For performance comparison, the following benchmarks are provided. 1) *RR w/o BD*: the RB index selected for each time slot and the beamforming vector at each available BS are both randomly generated. Note that this approach is supposed to be the worst, which may lead the DUE to suffer from the maximal transmission outage duration. 2) *RR w/ BD*: the RB index

scheduled for each time slot is randomly selected, but the beamforming vectors at available BSs are generated with the help of trained TD3 agent. 3) *RR w/ MRT*: different from *RR w/ BD*, MRT technique is invoked to generate the beamforming vectors, based on the corresponding estimated CSIs. 4) *ER w/ BD*: the RB index assigned for each time slot is the optimal via exhaustive search method, which can maximize (15) for every observed RBP map. Besides, the beamforming vector at each available BS is obtained from the trained TD3 agent. Note that this benchmark serves as the lower bound of EOD performance, which is supposed to help the DUE suffer the minimal transmission outage duration. 5) *ER w/ MRT*: different from *ER w/ BD*, the beamforming vectors are designed with the help of MRT technique, based on the corresponding estimated CSIs.

The proposed hybrid D3QN-TD3 solution provides the proper RB index for each time slot and designed beamforming vector for each available BS, with the aid of trained D3QN agent and TD3 agent, respectively. Fig. 10(a) and Fig. 10(b) show EOD curves of the proposed D3QN-TD3 solution and benchmarks versus P and M , respectively. It is clearly illustrated in Fig. 10(a) that the EOD curves decrease dramatically with the increase of P , which means that higher P can help the DUE achieve better transmission outage performance (i.e., lower EOD). Comparing the EOD curves of *RR w/o BD* and *RR w/ BD*, EOD performance enhancement can be observed (especially, for $P \in [-10, 40]$ dBm), which validates the effectiveness of TD3 component. Furthermore, via comparing the curves of *RR w/ BD* and *RR w/ MRT*, one can observe that the trained TD3 agent can help the UAV suffer from less amount of EOD than MRT beamforming scheme (for $P \in [-10, 40]$ dBm), in case of imperfect CSI estimation. Similar phenomenon can be observed via comparing *ER w/ BD* and *ER w/ MRT*. This is because the MRT beamforming strategy can only adapt to the estimated CSI, while the TD3 agent is trained to adapt to the overall imperfect CSI. Besides, greater EOD performance improvement can be achieved with the help of D3QN component, via comparing the EOD curves of *RR w/ BD* and the proposed hybrid D3QN-TD3 solution (especially, for $P \in [-20, 40]$ dBm). The aforementioned observations validate that the D3QN and TD3 agents are able to offer independent EOD performance gains, which is a remarkable feature of the proposed hybrid D3QN-TD3 solution. Compared to the optimal method *ER w/ BD*, the proposed hybrid D3QN-TD3 solution can help the DUE achieve sub-optimal EOD performance which performs slightly worse than the optimal approach but can provide significant EOD reduction than benchmarks *RR w/o BD*, *RR w/ BD* and *RR w/ MRT*. Most importantly, the proposed hybrid D3QN-TD3 solution outperforms *ER w/ MRT* as well, which means that

the joint RB allocation and beamforming design provided by the proposed hybrid D3QN-TD3 solution can offer more significant EOD reduction than that offered by MRT beamforming with optimal RB allocation. Similar conclusions can be drawn from Fig. 10(b) which demonstrates EOD curves versus various M . Note that for specific antenna number configuration, the proposed hybrid D3QN-TD3 algorithm needs to be retrained with the corresponding antenna number. From this figure, one can find the other fact that increasing M can help enhance EOD performance for solutions with beamforming design (*RR w/ BD*, *RR w/ MRT*, *Hybrid D3QN-TD3*, *ER w/ BD* and *ER w/ MRT*), but cannot achieve any EOD reduction for solution without beamforming design (*RR w/o BD*).

V. CONCLUSION

This paper studied a joint RB allocation and beamforming design optimization problem in a cellular-connected UAV network while protecting GUEs' transmission quality, in which the EOD of DUE was minimized via the proposed hybrid D3QN-TD3 algorithm. Specifically, the D3QN and TD3 agents were trained to accomplish the RB allocation in discrete action domain and beamforming design in continuous action regime, respectively. To realize this, an outer MDP was defined to characterize the dynamic RBP environment at the terrestrial BSs, while the inner MDP was formulated to trace the time-varying feature of B2D small-scale fading. The hybrid D3QN-TD3 solution was proposed to solve the outer MDP and the inner MDP interactively so that sub-optimal EOD performance for the considered optimization problem can be achieved. Numerical results illustrated that the proposed hybrid D3QN-TD3 solution can significantly reduce EOD for the DUE and achieve sub-optimal EOD performance, compared to the provided benchmarks. Most importantly, the trained D3QN and TD3 agents were also validated to offer independent improvements on EOD performance.

REFERENCES

- [1] L. Liu, S. Zhang, and R. Zhang, "Multi-beam UAV communication in cellular uplink: Cooperative interference cancellation and sum-rate maximization," *IEEE Trans. Wireless Commun.*, vol. 18, no. 10, pp. 4679–4691, 2019.
- [2] P. Chandhar, D. Danev, and E. G. Larsson, "Massive MIMO for communications with drone swarms," *IEEE Trans. Wireless Commun.*, vol. 17, no. 3, pp. 1604–1629, 2017.
- [3] Q. Wu, J. Xu, Y. Zeng, D. W. K. Ng, N. Al-Dhahir, R. Schober, and A. L. Swindlehurst, "A comprehensive overview on 5G-and-beyond networks with UAVs: From communications to sensing and intelligence," *IEEE J. Sel. Areas Commun.*, vol. 39, no. 10, pp. 2912–2945, 2021.

- [4] G. Hattab and D. Cabric, "Energy-efficient massive IoT shared spectrum access over UAV-enabled cellular networks," *IEEE Trans. Commun.*, vol. 68, no. 9, pp. 5633–5648, 2020.
- [5] Y. Li, A. H. Aghvami, and D. Dong, "Path planning for cellular-connected UAV: A DRL solution with quantum-inspired experience replay," *IEEE Trans. Wireless Commun.*, 2022.
- [6] F. Zhou, Y. Wu, H. Sun, and Z. Chu, "UAV-enabled mobile edge computing: Offloading optimization and trajectory design," in *Proc. IEEE Int. Conf. Commun. (ICC)*, Kansas, USA, 2018, pp. 1–6.
- [7] Z. Zhou, J. Feng, B. Gu, B. Ai, S. Mumtaz, J. Rodriguez, and M. Guizani, "When mobile crowd sensing meets UAV: Energy-efficient task assignment and route planning," *IEEE Trans. Commun.*, vol. 66, no. 11, pp. 5526–5538, 2018.
- [8] Z. Chu, W. Hao, P. Xiao, and J. Shi, "UAV assisted spectrum sharing ultra-reliable and low-latency communications," in *Proc. IEEE Global Commun. Conf. (GLOBECOM)*, Waikoloa, USA, 2019, pp. 1–6.
- [9] J. Hu, Y. Wu, R. Chen, F. Shu, and J. Wang, "Optimal detection of UAV's transmission with beam sweeping in covert wireless networks," *IEEE Trans. Veh. Technol.*, vol. 69, no. 1, pp. 1080–1085, 2019.
- [10] W. Wang, X. Li, M. Zhang, K. Cumanan, D. W. K. Ng, G. Zhang, J. Tang, and O. A. Dobre, "Energy-constrained UAV-assisted secure communications with position optimization and cooperative jamming," *IEEE Trans. Commun.*, vol. 68, no. 7, pp. 4476–4489, 2020.
- [11] G. Boudreau, J. Panicker, N. Guo, R. Chang, N. Wang, and S. Vrzic, "Interference coordination and cancellation for 4G networks," *IEEE Commun. Mag.*, vol. 47, no. 4, pp. 74–81, 2009.
- [12] C. Kosta, B. Hunt, A. U. Qudus, and R. Tafazolli, "On interference avoidance through inter-cell interference coordination (ICIC) based on OFDMA mobile systems," *IEEE Commun. Surveys Tuts.*, vol. 15, no. 3, pp. 973–995, 2012.
- [13] R. Zhang, Y.-C. Liang, and S. Cui, "Dynamic resource allocation in cognitive radio networks," *IEEE Signal Process. Mag.*, vol. 27, no. 3, pp. 102–114, 2010.
- [14] R. Irmer *et al.*, "Coordinated multipoint: Concepts, performance, and field trial results," *IEEE Commun. Mag.*, vol. 49, no. 2, pp. 102–111, 2011.
- [15] N. Senadhira, S. Durrani, X. Zhou, N. Yang, and M. Ding, "Uplink NOMA for cellular-connected UAV: Impact of UAV trajectories and altitude," *IEEE Trans. Commun.*, vol. 68, no. 8, pp. 5242–5258, 2020.
- [16] W. Mei, Q. Wu, and R. Zhang, "Cellular-connected UAV: Uplink association, power control and interference coordination," *IEEE Trans. Wireless Commun.*, vol. 18, no. 11, pp. 5380–5393, 2019.
- [17] Y. Zeng, X. Xu, S. Jin, and R. Zhang, "Simultaneous navigation and radio mapping for cellular-connected UAV with deep reinforcement learning," *IEEE Trans. Wireless Commun.*, vol. 20, no. 7, pp. 4205–4220, 2021.
- [18] X. Wang, M. C. Gursoy, T. Erpek, and Y. E. Sagduyu, "Jamming-resilient path planning for multiple UAVs via deep reinforcement learning," in *Proc. IEEE Int. Conf. Commun. Workshops (ICC Workshops)*, Montreal, 2021, pp. 1–6.
- [19] R. Ding, F. Gao, and X. S. Shen, "3D UAV trajectory design and frequency band allocation for energy-efficient and fair communication: A deep reinforcement learning approach," *IEEE Trans. Wireless Commun.*, vol. 19, no. 12, pp. 7796–7809, 2020.
- [20] P. Series, "Propagation data and prediction methods required for the design of terrestrial broadband radio access systems operating in a frequency range from 3 to 60 GHz," *Recommendation ITU-R*, pp. 1410–1415, 2013.
- [21] Z. Yang, C. Pan, K. Wang, and M. Shikh-Bahaei, "Energy efficient resource allocation in UAV-enabled mobile edge computing networks," *IEEE Trans. Wireless Commun.*, vol. 18, no. 9, pp. 4576–4589, 2019.
- [22] 3GPP TR 36.777, "Enhanced LTE support for aerial vehicles," Dec. 2017.
- [23] H. Joudeh and B. Clerckx, "Sum-rate maximization for linearly precoded downlink multiuser MISO systems with partial CSIT: A rate-splitting approach," *IEEE Trans. Commun.*, vol. 64, no. 11, pp. 4847–4861, 2016.

- [24] J. Choi, "Joint rate and power allocation for NOMA with statistical CSI," *IEEE Trans. Commun.*, vol. 65, no. 10, pp. 4519–4528, 2017.
- [25] L. Xiao, Y. Ding, J. Huang, S. Liu, Y. Tang, and H. Dai, "UAV anti-jamming video transmissions with QoE guarantee: A reinforcement learning-based approach," *IEEE Trans. Commun.*, vol. 69, no. 9, pp. 5933–5947, 2021.
- [26] T. P. Lillicrap, J. J. Hunt, A. Pritzel, N. Heess, T. Erez, Y. Tassa, D. Silver, and D. Wierstra, "Continuous control with deep reinforcement learning," in *Proc. of ICLR*, 2015.
- [27] Y. Li, R. Zhao, Y. Deng, F. Shu, Z. Nie, and A. H. Aghvami, "Harvest-and-opportunistically-relay: Analyses on transmission outage and covertness," *IEEE Trans. Wireless Commun.*, vol. 19, no. 12, pp. 7779–7795, 2020.